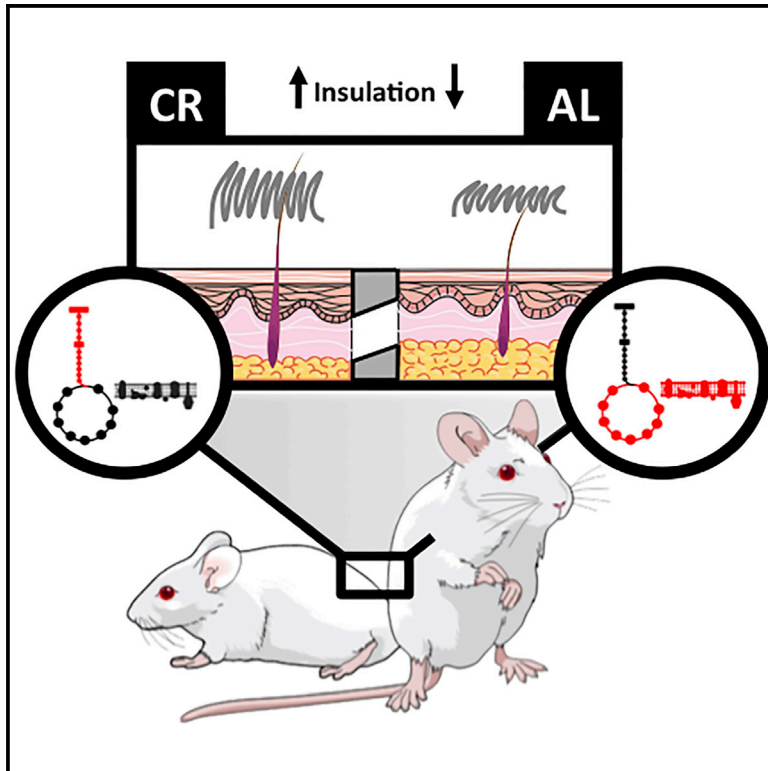


# Cell Reports

## Caloric Restriction Promotes Structural and Metabolic Changes in the Skin

### Graphical Abstract



### Authors

Maria Fernanda Forni, Julia Pelligia, Tarcio T. Braga, ..., Carlos Arturo Navas, Niels Olsen Saraiva Camara, Alicia J. Kowaltowski

### Correspondence

alicia@iq.usp.br

### In Brief

Caloric restriction significantly increases the lifespan, but its effect on the skin is poorly understood. Forni et al. show that caloric restriction changes the structure and metabolism of the skin; these changes affect whole-body thermoregulation.

### Highlights

- Caloric restriction (CR) remodels the skin and fur and expands the local stem cell pool
- CR promotes metabolic reprogramming in both the dermis and epidermis
- CR imposes a thermoregulatory challenge in the absence of fur
- Changes in CR fur are necessary for thermal homeostasis and metabolic fitness



# Caloric Restriction Promotes Structural and Metabolic Changes in the Skin

Maria Fernanda Forni,<sup>1</sup> Julia Peloggia,<sup>1</sup> Tarcio T. Braga,<sup>2</sup> Jesús Eduardo Ortega Chinchilla,<sup>3</sup> Jorge Shinohara,<sup>4</sup> Carlos Arturo Navas,<sup>3</sup> Niels Olsen Saraiva Camara,<sup>2</sup> and Alicia J. Kowaltowski<sup>1,5,\*</sup>

<sup>1</sup>Departamento de Bioquímica, Instituto de Química, Universidade de São Paulo, Av. Prof. Lineu Prestes, 748, 05508-000 São Paulo, Brazil

<sup>2</sup>Instituto de Ciências Biomédicas, Universidade de São Paulo. Av. Prof. Lineu Prestes, 1730, 05508-900 São Paulo, Brazil

<sup>3</sup>Departamento de Fisiologia, Instituto de Biologia, Universidade de São Paulo, R. do Matão, 321, 05508-090 São Paulo, Brazil

<sup>4</sup>Laboratório de Química Supramolecular e Nanotecnologia – LQSN, Instituto de Química, Universidade de São Paulo, Av. Prof. Lineu Prestes, 748, 05508-000 São Paulo, Brazil

<sup>5</sup>Lead Contact

\*Correspondence: [alicia@iq.usp.br](mailto:alicia@iq.usp.br)

<http://dx.doi.org/10.1016/j.celrep.2017.08.052>

## SUMMARY

Caloric restriction (CR) is the most effective intervention known to enhance lifespan, but its effect on the skin is poorly understood. Here, we show that CR mice display fur coat remodeling associated with an expansion of the hair follicle stem cell (HFSC) pool. We also find that the dermal adipocyte depot (dWAT) is underdeveloped in CR animals. The dermal/vennule annulus vasculature is enlarged, and a vascular endothelial growth factor (VEGF) switch and metabolic reprogramming in both the dermis and the epidermis are observed. When the fur coat is removed, CR mice display increased energy expenditure associated with lean weight loss and locomotion impairment. Our findings indicate that CR promotes extensive skin and fur remodeling. These changes are necessary for thermal homeostasis and metabolic fitness under conditions of limited energy intake, suggesting a potential adaptive mechanism.

## INTRODUCTION

Aging involves the progressive accumulation of deleterious changes in cells and tissues over time, leading to increased disease and death risks as well as decreased fitness in almost all organisms (López-Otín et al., 2013). Many of these age-related changes can be prevented by caloric restriction (CR), a dietary intervention that extends lifespan and improves healthspan in a variety of species through the limitation of dietary calories without a lack of essential nutrients (Sohal and Weindruch, 1996; Partridge and Gems, 2002; Roth et al., 2004). Most mammalian studies investigating CR are conducted using laboratory rodents and have uncovered multiple metabolic effects of CR in the brain, heart, liver, adipose tissue, and skeletal muscle, including changes in oxidative phosphorylation, protein and lipid storage, and turnover (Speakman and Mitchell, 2011).

Although CR has been extensively studied regarding its effects on many major organs, no study to date has focused on its

functional and metabolic effect on the skin. Studies of this are important because the skin is the largest mammalian organ and acts as a primary barrier against heat loss, dehydration, mechanical trauma, and microbial insults (Watt, 2014; Fuchs, 2015). As a result, the skin and its appendages, such as hair follicles (HFs), would be expected to be important in adaptations to stimuli such as dietary interventions with an effect on aging.

Interestingly, studies involving the effects and mechanisms of CR using mice are conducted with animals housed under typical laboratory conditions, including temperatures markedly below thermoneutrality (Nedergaard and Cannon, 2013; Romanovsky, 2014). Under these conditions, metabolic rates increase greatly, and animals depend more on their insulation capacity (Nedergaard and Cannon, 2013). Thus, CR studies showing that this dietary intervention promotes life- and healthspan extension were conducted in situations in which the structural and functional characteristics of the skin and fur are particularly important. This study was designed to uncover how CR affects the skin and fur under typical laboratory animal conditions. Our findings indicate not only that CR promotes extensive skin and fur remodeling but show that this remodeling is critical for metabolic fitness under conditions of limited energy intake.

## RESULTS

### CR Remodels the Fur Coat

We calorically restricted mice for 6 months, a time span sufficient to observe many of the metabolic phenotypes associated with this diet (McDonald and Ramsey, 2010). Consistent with prior reports (Bruss et al., 2011), CR mice presented a 54% decrease in body mass gain after this 6-month treatment and were considerably smaller compared with ad libitum (AL)-fed counterparts (Figure 1A; Figures S1A–S2C). CR animals also visibly displayed more even, thick, and long back skin fur coats (Figure 1B). To evaluate the composition of the fur coat, we quantified the four types of hair follicles in the back skin; namely, awl, Auchenne, zigzag, and guard. Awl hairs are straight and shorter than guard hairs, contain three or four medulla cell rows, and form in the second wave of hair morphogenesis at embryonic day 15 (E15)–E16.5 (Müller-Röver et al., 2001; Driskell et al., 2011). Their numbers were unaltered in CR animals, but they presented less dispersion between CR individuals (Figure 1C). Auchenne hairs

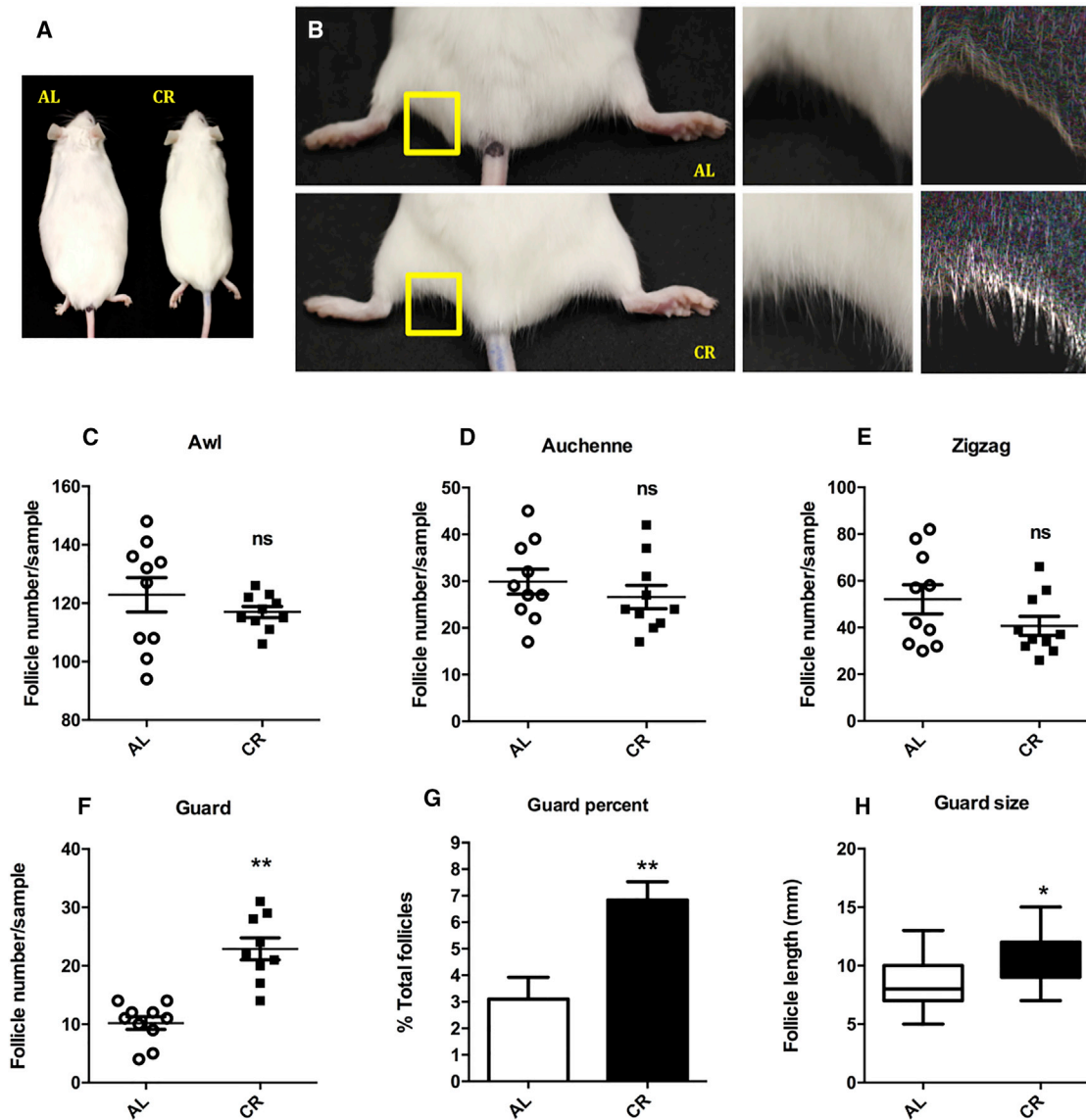


**Figure 1. Long-Term CR Promotes Fur Remodeling**

(A) Representative images of ad libitum (AL)-fed and calorically restricted animals (60% food intake AL).

(B) Higher magnification of the fur coat.

(C–F) Four different types of hair follicles were sampled and categorized as described in the [Experimental Procedures](#): (C) awl, (D) Auchenne, (E) zigzag, (F) guard.

(G) Guard follicles quantified as the percentage of total follicles.

(H) Guard length.

n = 2 independent experiments with 5 animals per group (10 animals). Data represent means ± SEM. \*p ≤ 0.05; \*\*p ≤ 0.001; ns, not significant relative to AL.

are similar to awl hairs, except they have one kink in the hair shaft (Müller-Röver et al., 2001), and were present in equal quantities in the AL and CR groups (Figure 1D). The same lack of change was observed for zigzag hairs (Figure 1E), which present one row of medulla cells and at least two bends in the hair shaft, granting the characteristic “Z” shape. Guard hairs, the longest, do not have kinks and develop during the first wave of hair follicle morphogenesis at E13–E14.5 (Schlake, 2007). Despite their low frequency, guard hairs presented highly increased density in CR animals (Figure 1F; p ≤ 0.001), doubling the quantities seen in AL

mice. This reflects a significant change in the percentage of guard hairs, which was 2%–4% in AL animals and 6%–8% in CR animals (Figure 1G; p ≤ 0.001). Importantly, not only their numbers but also their length was increased in CR animals (Figure 1H; p ≤ 0.05). These changes were specific to CR animals and were not observed in AL animals matched for CR animal size (Figure S2).

Overall, we characterized phenotypic alterations and a remodeled back skin fur coat coverage in CR. The growth of these hair shafts is sustained by hair follicle stem cells (HFSCs) (Hsu et al.,

2014), so our next step was to investigate whether CR affected epidermal stem cells.

### CR Enlarges the Hair Follicle Stem Cell Pool and Promotes Higher Hair Follicle Growth and Retention Rates

Epidermal and hair follicle stem cells are responsible for the maintenance of both the interfollicular epidermis as well as hair follicles. To estimate the pool of CD29+ interfollicular and CD34+/ $\alpha$ 6integrin<sup>HIGH</sup> hair follicle stem cells (Cotsarelis, 2006; Arwert et al., 2012), we assessed their relative numbers using flow cytometry. We found an overall increase in interfollicular stem cells in CR animals (Figures 2A and 2B;  $p \leq 0.05$ ) and also an increase in the number of hair follicle stem cells associated with the bulge (Figures 2C and 2D;  $p \leq 0.05$ ), which promotes hair follicle maintenance and growth.

We asked next whether these expanded pools of stem cells lead to stimulated hair growth rates. This was addressed by clipping the fur off the back skin of AL and CR animals and evaluating the regrowth rate (Figures 2E and 2F). Two weeks after this procedure, the percentage of the original area covered with new fur was much larger in CR mice (Figures 2E and 2F;  $p \leq 0.001$ ). This tendency was maintained until the last measured time point (4 weeks), when CR animals displayed full coverage of the initial area. A further indicator of the higher growth rates displayed in CR animals is the area under the curve shown in Figure 2F, almost double that for AL (Figure 2G;  $p \leq 0.001$ ). We also evaluated whether hair shaft maintenance is affected by CR. This was measured by dyeing the back skin area and evaluating the color dilution because of the substitution of lost follicles over 28 weeks (representative photos and an in-depth color palette are shown in Figure 2H). Surprisingly, CR animals presented much less hair shaft loss and lower substitution rates, a fact made evident by the maintenance of the area that remained colored over time (Figures 2I and 2J;  $p \leq 0.001$  and 0.05, respectively). This may be due to the fact that calorie shortage imposed by CR can act as a mechanism to conserve energy, delaying entry into catagen/telogen or the resting phase when hair is released (Müller-Röver et al., 2001).

### CR Thickens the Epidermis, Decreases Dermal White Adipose Tissue, and Enlarges the Vascular Network

Next, we investigated whether CR induces morphologic or ultrastructural alterations in the skin that accompany the changes seen in the fur. Skin histology sections (Figure 3A) clearly demonstrate that tissue ultrastructure is modified by prolonged CR. Epidermal thickness was more than double in CR mice, reminiscent of young tissue (Figure 3B;  $p \leq 0.001$ ). Conversely, AL animals displayed thick dermal white adipose tissue (dWAT) (Driskell et al., 2014; Alexander et al., 2015; Kasza et al., 2014), contrasting with that observed in the CR group (Figure 3B,  $p \leq 0.001$ ). This result is expected because this tissue is a fat depot that stores excess energy.

CR has also been shown to improve angiogenesis and vessel sprouting in a vascular endothelial growth factor (VEGF)-dependent manner (Hoeben et al., 2004). To investigate whether this was true for dermis-associated vasculature, we evaluated circulating levels of murine VEGF (mVEGF) and found no significant

differences between AL and CR animals (Figure 3D). The same lack of difference was observed in the epidermis (Figure 3E). Nonetheless, the relative levels of mVEGF were almost three times higher in the dermal compartment of CR animals (Figure 3F;  $p \leq 0.001$ ). Because the main physiological function of mVEGF is to induce capillary sprouts, dermis-associated vasculature was evaluated by measuring CD31+ endothelial cells (Liu and Shi, 2012). The relative numbers of CD31+ cells around the bulge are indicative of venule annules capillaries, responsible for nutrient transport to the hair follicle stem cell niche. We found that these cells were increased in CR animals (Figure 3G;  $p \leq 0.05$ ). Accordingly, the relative area covered by CD31+ cells in the dermis was also increased (Figure 3H;  $p \leq 0.001$ ). More importantly, after intravenous injection of a dye, the area covered by the capillary net in the dermis was found to be increased (Figure 3I;  $p \leq 0.05$ ; digital mapping of the number of pixels per circulatory branch area). These data collectively suggest that the vasculature compartment is expanded in CR skin.

Because enlarged vasculature is associated with higher metabolic substrate availability (Hoeben et al., 2004), we hypothesized that CR could affect dermal and epidermal metabolism.

### CR Leads to Metabolic Reprogramming in Both the Epidermis and Dermis

How adult tissue stem cells metabolically respond to the nutritional state of the whole organism is not well known (Mihaylova et al., 2014). In differentiated cells, many studies demonstrate that CR stimulates respiratory rates by increasing organelle numbers or mass (mitochondrial biogenesis; Nisoli et al., 2004; Guarente, 2008). To assess the effect of CR on skin metabolism, we evaluated O<sub>2</sub> consumption rates in intact primary cells derived from both the epidermis and the dermis. To do this, the epidermal sheet was separated from the dermis, and both were enzymatically digested and mechanically dissociated into single cells, generating primary cultures (Forni et al., 2016).

Real-time O<sub>2</sub> consumption rates (OCRs) in CR epidermal primary cell cultures show that basal respiration (which represents the sum of all physiological mitochondrial O<sub>2</sub>-consuming processes) was decreased in the epidermal compartment, indicating lower respiratory function compared with AL animals (Figure 4A shows typical epidermis time scans quantified in subsequent panels; Figure 4B;  $p \leq 0.001$ ).

The injection of oligomycin (oligo), an ATP synthase inhibitor, leads to a decrease in basal respiration that is reflective of O<sub>2</sub> consumption used to generate ATP (Figure 4C). In addition to low basal respiration, CR epidermal cells presented a very low ATP-linked OCR (Figure 4C;  $p \leq 0.001$ ), indicating a small contribution of mitochondria toward ATP generation in these cells.

The addition of carbonyl cyanide-p-trifluoromethoxy-phenylhydrazone (CCCP) uncouples respiration from oxidative phosphorylation and allows for the measurement of maximal OCR (Figure 4D), which was lower in CR epidermal cells (Figure 4D;  $p \leq 0.001$ ), indicating lower overall mitochondrial activity. The spare respiratory capacity, calculated by subtracting CCCP-stimulated from basal OCR, was not significantly different in AL and CR epidermal cultures (Figure 4E). The proton leak, or non-mitochondrial respiration subtracted from the post-oligomycin injection OCR, is associated with the proton leak across

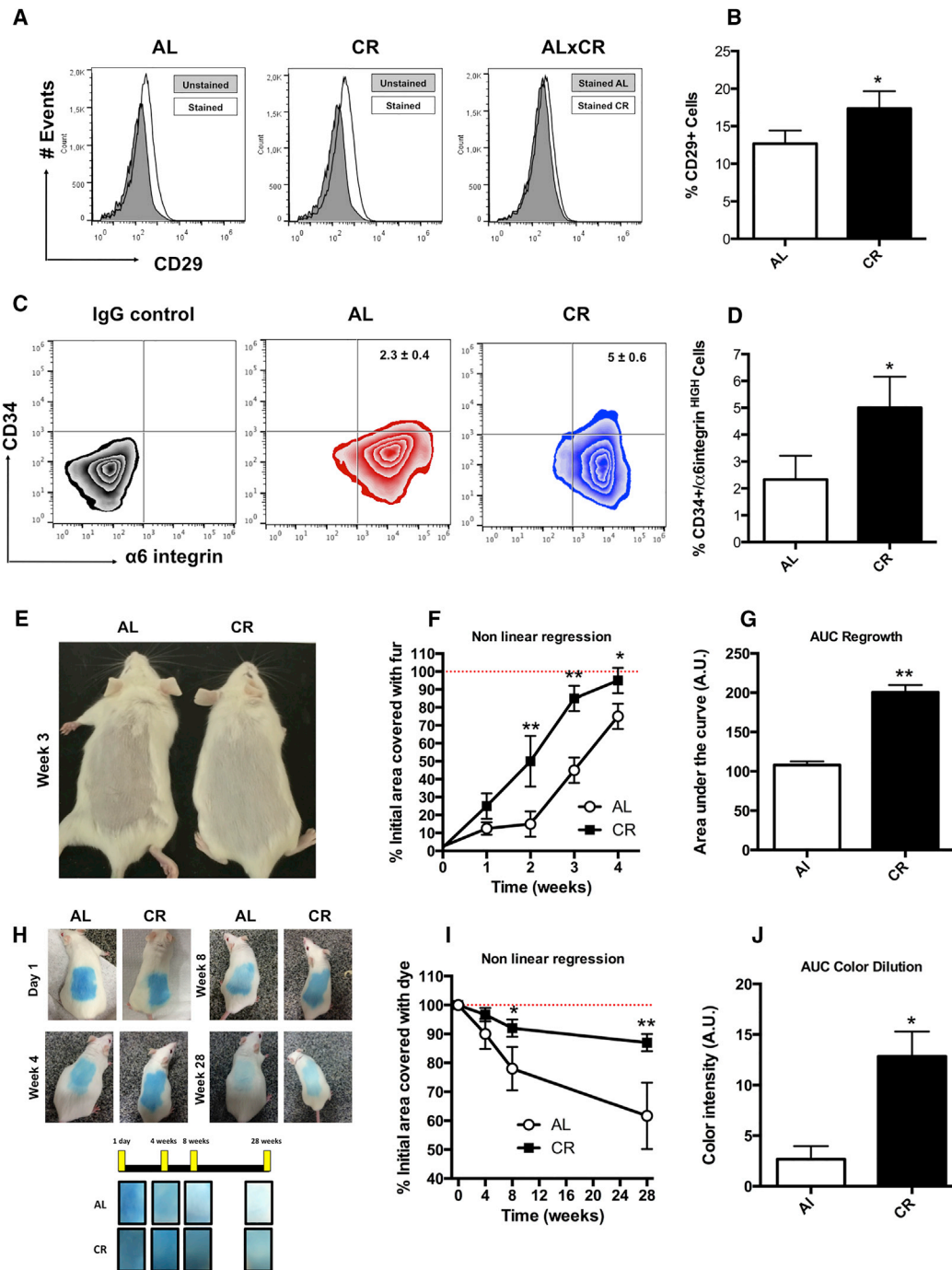


**Figure 2. CR Increases Epidermal Stem Cell Pools and Enhances Fur Growth**

(A) Representative histograms of CD29<sup>+</sup> interfollicular stem cell populations estimated through flow cytometry.

(B) Quantification of the data in (A).

(C) Representative dot blots of CD34<sup>+</sup>/α6 integrin<sup>HIGH</sup> hair follicle stem cells estimated through flow cytometry.

(D) Quantification of the data in (C).

(E) Hair follicle growth after removal; representative image.

(F and G) Hair follicle growth after removal and back skin regrowth area quantification (F) and area under the curve of (F) (G).

(H) Hair maintenance evaluated through back skin fur dye dilution; representative images.

(I and J) Hair maintenance quantification (I) and area under the curve (J).

n = 4 independent experiments with 5 animals per group (20 animals). Data are representative of mean ± SEM. \*p ≤ 0.05, \*\*p ≤ 0.001. At least 50,000 events per point were collected for the flow cytometry experiments.

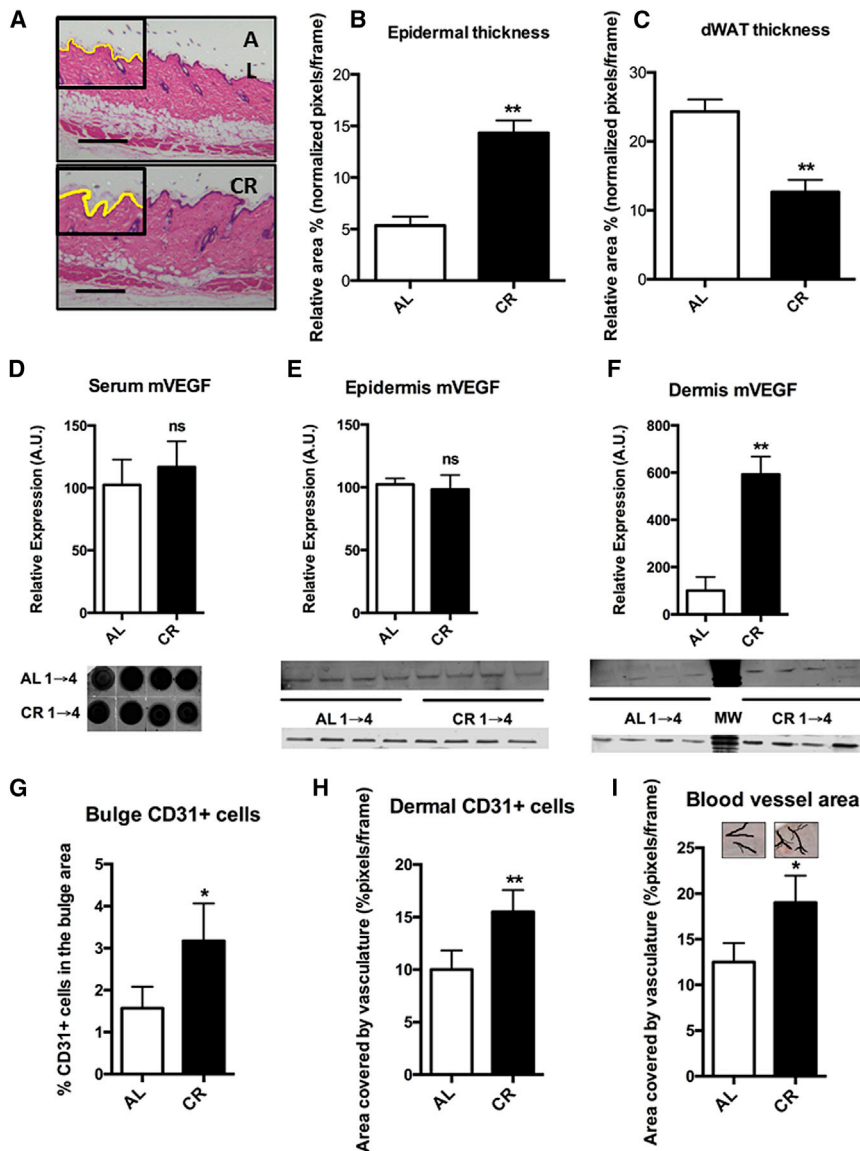


### Figure 3. CR Induces Morphologic and Ultrastructural Alterations in the Skin

(A) Skin ultrastructure visualized using H&E histochemistry. (B and C) Relative areas of the epidermis (B) and dWAT (C) were quantified. (D–F) The relative levels of murine VEGF were evaluated by western blotting the serum (D), epidermis (E), and dermis (F). (G) Hair follicle vasculature (vennule annulus) was estimated through CD31+ cell quantification in the bulge area in immunofluorescence experiments. (H and I) Dermal vasculature was estimated through (H) CD31+ cell quantification in whole-mount dermal preparations and (I) digital quantification using manually drawn pixel masks over the area that presented veins and capillaries filled with an intravenously loaded dye. n = 4 independent experiments with 5 animals per group (20 animals). Data are representative of means ± SEM. \*p ≤ 0.05, \*\*p ≤ 0.001. The scale bars in (A) represent 200 μm.

Thus, the CR dermis displays an enhanced respiratory phenotype, and cells are highly dependent on mitochondria for ATP generation. Moreover, both maximal and spare respiratory capacities were considerably increased (Figures 4L and 4M; p ≤ 0.001), indicating an expansion of the mitochondrial network content per cell. H<sup>+</sup> leak-induced respiration was decreased in CR dermal cells (Figure 4N; p ≤ 0.05), suggesting that a high percentage of the protons pumped toward electron transport chain complexes return to the matrix through ATP synthase, maximizing ATP production. Finally, non-mitochondrial respiration (Figure 4O; p ≤ 0.001) and ECAR (Figure 4P; p ≤ 0.001) were significantly increased in CR dermal cells. Citrate synthase activity, which correlates with mitochondrial mass, did not display significant differences between the two groups in the epidermis. A stark difference was observed in the dermis, where the relative enzymatic activity presented by CR animals was more than double that of the AL group (Figures S3A and S3B). These observations support the previous notion that mitochondrial function is enhanced by CR mainly in the dermis.

the inner mitochondrial membrane independent of ATP synthase activity. This rate was significantly increased in CR epidermal cells (Figure 4F; p ≤ 0.001), demonstrating that the lack of ATP-linked respiration is not only due to the lower maximal respiratory capacity but also due to a decrease in coupling. Finally, the extent of non-mitochondrial oxygen-consuming processes was estimated by inhibiting the respiratory chain with antimycin A and rotenone (Figure 4G). Non-mitochondrial respiration accounted for a small fraction of cellular OCR but was significantly lower in CR epidermis (Figure 4G; p ≤ 0.001). The extracellular acidification rate (ECAR), an indirect measurement of lactate production and secretion, was also measured and found to be unaltered (Figure 4H).

An entirely different metabolic response to CR was observed in the dermis (Figure 4I). CR dermal cells displayed not only substantially enhanced basal OCRs (Figure 4J; p ≤ 0.001) but also higher ATP production-dependent respiration (Figure 4K; p ≤ 0.05).

relates with mitochondrial mass, did not display significant differences between the two groups in the epidermis. A stark difference was observed in the dermis, where the relative enzymatic activity presented by CR animals was more than double that of the AL group (Figures S3A and S3B). These observations support the previous notion that mitochondrial function is enhanced by CR mainly in the dermis.

Overall, the metabolic shift in the two most important skin compartments, added to the expanded vasculature and changes in the fur, suggests that CR animals may present very different thermoregulatory properties. To investigate this, we analyzed heat loss in AL and CR mice.

### Fur Coat Remodeling Improves Thermoregulatory Properties in CR Animals

We hypothesized that changes in fur coats observed in CR animals could be related to thermoregulation and used an infrared

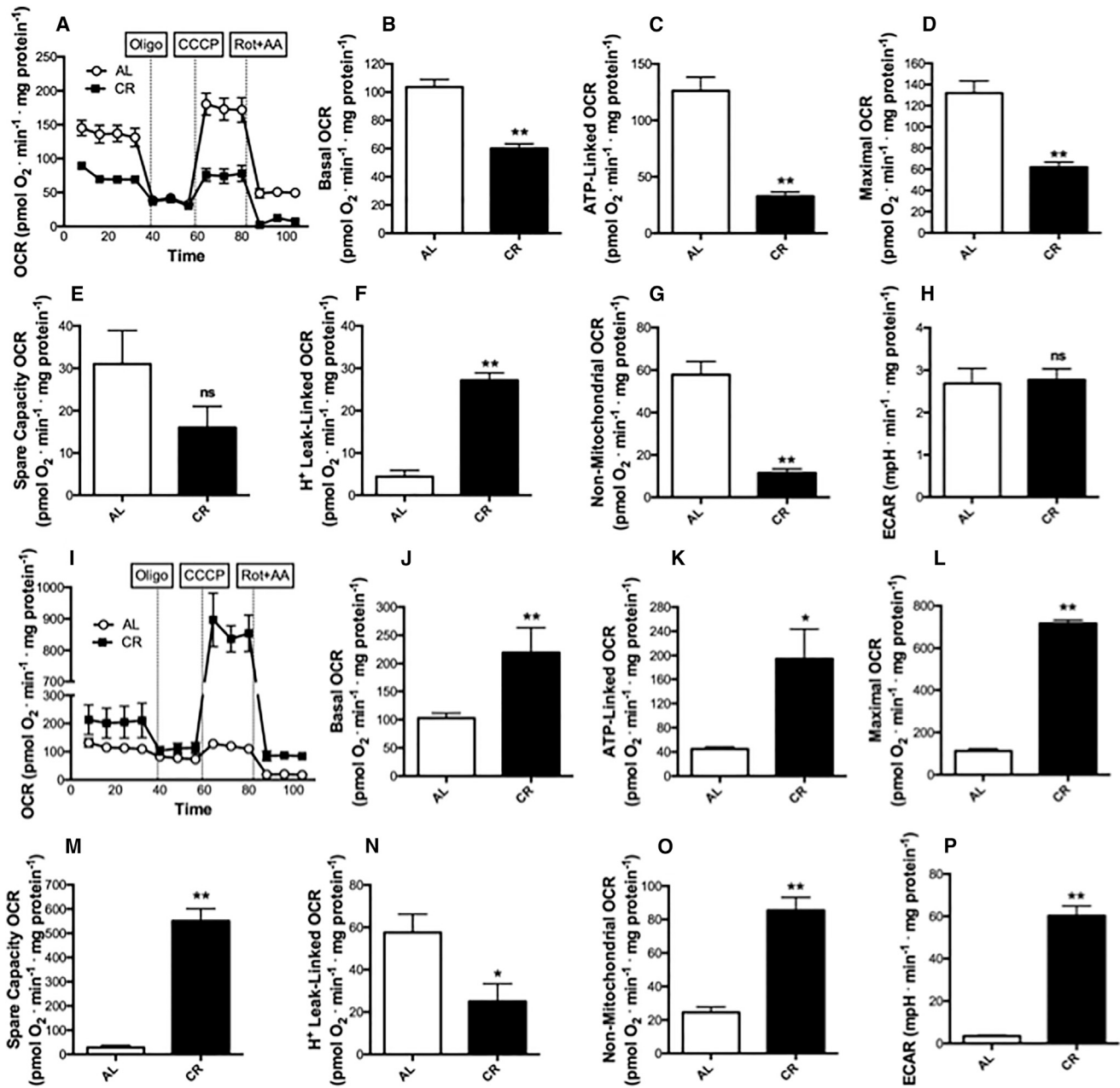


**Figure 4. CR Decreases Oxidative Metabolism in the Epidermis and Increases It in the Dermis**

(A) Real-time whole-cell epidermis  $O_2$  consumption rates (OCRs) were measured in AL (○) and CR (■) animal-derived primary epidermal cultures. Oligomycin, CCCP, and rotenone plus antimycin A were added, where indicated, at the concentrations described in the [Experimental Procedures](#).

(B–G) Basal  $O_2$  consumption rates (B), ATP-production dependent OCR (C), maximal OCR (D), spare respiratory capacity (E),  $H^+$  leak-linked OCR (F), and non-mitochondrial respiration (G) were derived from data such as those shown in (A).

(H) Extracellular acidification rates.

(I) Real-time whole-cell dermis OCRs were measured in AL (○) and CR (■) animal-derived primary dermal cultures. Oligomycin, CCCP, and rotenone plus antimycin A were added where indicated.

(J–O) Basal  $O_2$  consumption rates (J), ATP-production dependent OCR (K), maximal OCR (L), spare respiratory capacity (M),  $H^+$  leak-linked OCR (N), and non-mitochondrial respiration (O) were derived from data such as those shown in (J).

(P) Extracellular acidification rates.

n = 3 independent experiments with 5 animals per group (15 animals). \*p ≤ 0.05, \*\*p ≤ 0.001.

thermal imaging system to capture the surface temperatures of both AL and CR animals (Figure 5A). No significant differences were observed between the AL and CR groups when the back skin fur coat was present, indicating that CR animals maintain a body surface temperature similar to AL animals. However, when the same individuals were imaged after clipping the dorsal body surface fur, CR animals presented significantly higher heat loss ( $p \leq 0.001$ ; quantifications are shown in Figure 5A, right). This result indicates that the remodeled fur substantially contributes toward thermoregulation in CR animals.

Our infrared thermal imaging experiments lead us to hypothesize that CR animals display a coat with a higher insulating capacity. In mammals, a layer of air is trapped between the surface of the skin and the outer surface of the hair coat, and the degree of insulation can be altered by increasing or decreasing the thickness of the air layer (Hart, 1956). To measure whether the CR-remodeled fur coat had better insulating properties, we developed an Arduino-based system to simultaneously record the temperature below (bottom) and above (top) the hair coat (Figure 5B). Representative experimental traces are shown in Figure 5C for both groups. The differences between body heat that reaches the epidermis (bottom data) and the temperature at the hair surface (top) are significantly larger in the CR group (blue lines), suggesting that heat is more efficiently trapped by CR pelage. Moreover, a slight increase over time in the temperature of the fur coat surface in the AL group (top, red line) indicates that this pelage is more leaky than that of the CR group (Figure 5C). The average difference in temperature between the body surface and hair coat surface is shown in Figure 5D and, despite large individual variability, showed a trend for CR fur to display a higher difference relative to the AL group ( $p = 0.057$ ). These observations again suggest that CR fur coats presents better insulating properties compared with the AL group.

The same system was coupled to a device measuring thermal conductivity across a section of dissected back skin to measure *ex vivo* differences in both intact skin plus fur and shaved skin (Figure 5E), a setting that decreased variability between individual samples. We saw a significant decrease in shaved CR skin temperature differences relative to shaved AL skin ( $p < 0.05$ ), indicating that changes in skin thickness and composition under this dietary intervention make it less insulating. Notably, the difference in temperatures, comparing conditions with and without fur, in CR samples was much larger than in AL samples, a result in line with the increased thermal isolation of the CR fur coat seen in *in vivo* experiments (Figure 5E;  $p \leq 0.001$ ). These results confirm that CR promotes an increase in fur coat insulation.

An additional factor in mammalian thermoregulation is dermal blood flow, which is regulated to ensure that the difference in temperature between the skin surface and the environment remains constant, transporting heat from the body core to the surface (Terrien et al., 2011). We assessed the vasculature in the dermis in shaved CR and AL animals using a laser Doppler apparatus before and after epinephrine stimulation. Basal blood flow was increased in the CR group (Figure 5F;  $p \leq 0.05$ ), indicating that the dermal vasculature in this group presents a decreased degree of vasoconstriction relative to that expected, given that the absence of fur elicits a cold-induced response. After an acute stimulus with epinephrine, blood flow increased

to equal levels in both groups. Recovery to basal levels was observed in AL but not CR animals. Overall, vasoconstriction appeared to be impaired in the CR group, as well as recovery capacity (Figure 5G;  $p \leq 0.001$ ). These alterations may further contribute to the loss of heat observed in shaved CR animals relative to AL animals.

Because typical laboratory animal housing conditions are below thermoneutrality (Cannon and Nedergaard, 2011; Romanovsky, 2014), the energy spent on thermoregulation could be a metabolic burden for CR mice, regulated by fur remodeling. We thus asked what the effect of fur on global metabolic parameters is and how CR affects this.

### Fur Removal Leads to Metabolic and Locomotion Impairment in CR Animals

Whole-body energy metabolism can be evaluated in live mammals by measuring metabolic processes that generate heat through indirect calorimetry, following the amount of  $O_2$  consumed (Speakman, 2013). The data shown in Figures 6A and 6B (black lines) show that CR mice present lower  $O_2$  consumption ( $VO_2$ ) rates relative to AL animals, as expected because of their smaller body size. Both AL and CR mice with fur maintained constant  $VO_2$  rates over the 24-hr period. A higher  $VO_2$  was observed in both groups after back skin hair clipping (Figures 6A and 6B, blue lines) but with different patterns: although the AL group presented constant levels of increased  $VO_2$  throughout the light/dark cycle (Figure 6A, blue line), the CR group displayed higher  $VO_2$  values during the first hours of the dark cycle, which may indicate higher use of lipids as an energy source (lipids are more reduced). Interestingly, the levels of both lactate and urea were increased in shaved CR animals 4 hr after the beginning of the dark period (Figures S3C and S3D), suggesting that protein degradation and lactate formation occur in the CR group.

Heat released was relatively lower both in AL and CR animals with fur (Figures 6C and 6D, black lines), and hair removal led to increased energy expenditure in both groups (24% in the AL group, 40% in the CR group; Figures 6C and 6D, blue lines). Spontaneous physical activity (SPA) levels in AL animals were, as expected (Oelkrug et al., 2015), higher during the dark period and not changed by fur removal (Figure 6E). As described previously (Lusseau et al., 2015), CR animals with fur presented the same ambulatory pattern whether in the dark or light (Figure 6F, black line), with increased overall movement compared with AL animals. When their fur coat was removed, the movement pattern was disrupted, and CR animals spent substantial time periods with very low spontaneous activity (yellow arrows, Figure 6F, blue line; the blue line in Figure 6G shows individual shaved CR animal spontaneous movement traces for identification of the low-movement periods). Indeed, these animals were probably in a state of torpor because marked heat production decreases were also observed during these periods (a heat and SPA overlay for individual animals is shown in Figure 6G).

Whole-body metabolic assays in AL versus CR animals may, however, present differing results because of the smaller body size of CR animals. To explore this possibility, we used body size/weight-matched younger AL animals (Figure S4). We failed

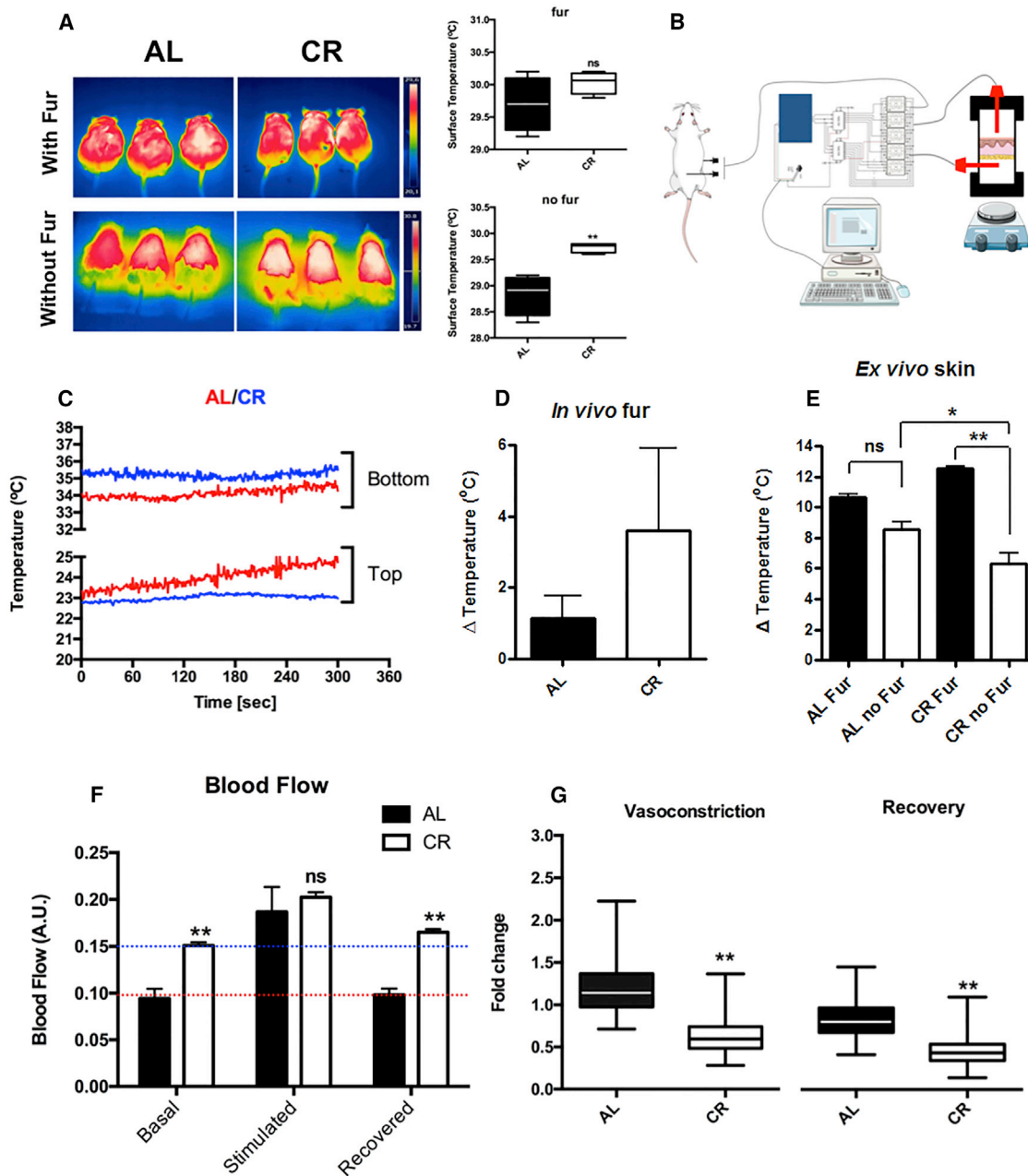


### Figure 5. CR Fur Is Highly Insulating

(A) IR thermal imaging was used to capture the surface temperatures of AL and CR animals with fur or after removing the back skin fur coat. Right: surface temperature quantifications with and without fur, as indicated.  $n = 3$  independent experiments with 5 animals per group (15 animals).  $**p \leq 0.001$ .

(B) An Arduino-based system was developed to simultaneously record temperatures below and above the hair coat.

(C) Representative traces for the AL and CR groups.

(D) Quantification of in vivo fur thermal isolation measurements.

(E) The same system was coupled to a device measuring the temperature at a heat source and in the environment just above the skin to evaluate heat transfer across an ex vivo section of dissected skin. These measurements were performed with and without fur and quantified as differences in temperatures.

(F) A laser Doppler probe was used to record real-time mean blood flow at 1-s intervals. After monitoring for 300 s, epinephrine ( $0.1 \mu\text{g}$  in  $20 \mu\text{l}$ ) was subcutaneously applied approximately 3 cm away from the probe site, and 100 s were recorded as the stimulated period. The remaining 200 s were recorded as the recovery period. Shown are segments from blood flow recording designated as basal (blue line), relating to the unstimulated period.

(G) Vasoconstriction index (stimulated/basal) and recovery capacity (recovered/basal).

The data represent averages  $\pm$  SEM and were compared using t tests (4–6 animals).  $*p < 0.05$ ,  $**p < 0.01$  versus AL.

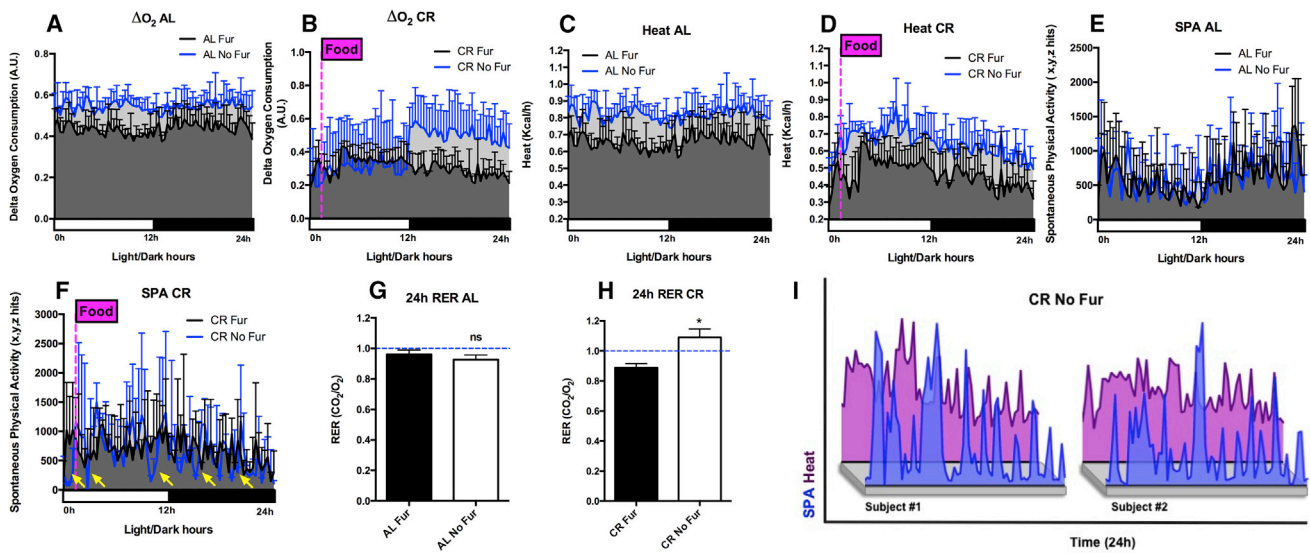


**Figure 6. CR Animals Depend on Fur to Maintain Metabolic and Ambulatory Fitness**

Indirect calorimetry was employed to assess whole-body metabolism, heat production, and locomotion patterns of AL and CR animals with fur (black lines) or after removing the back skin fur coat (blue lines).

(A and B) AL (A) and CR (B)  $O_2$  consumption ( $VO_2$ ).

(C and D) AL (C) and CR (D) heat production (kilocalories per hour).

(E and F) AL (E) and CR (F) spontaneous physical activity (SPA; combined hits on the x, y, and z axes).

(G) An overlay of individual SPA (blue) and heat (pink) measurements showing simultaneous decreases in both parameters.

$n = 2$  independent experiments with 5 animals per group (10 animals). \* $p \leq 0.05$ , \*\* $p \leq 0.001$ .

to observe any similarities in  $VO_2$ , heat, or SPA patterns between body size-matched and CR animals (Table S1).

Overall, fur removal seems to promote substantial changes in whole-body metabolic rates for AL and CR animals, with more energy expenditure in CR animals. We thus decided to evaluate the effect of prolonged fur absence.

### Fur-Deprived CR Mice Lose Lean Mass, whereas Shaved AL Animals Mobilize Fat

Because our results show that the lack of fur imposes different thermoregulatory demands in AL and CR animals, we decided to evaluate the role of prolonged fur absence (1 month) on metabolic maintenance in animals. Our first observation was that the absence of fur imposes a significant metabolic challenge for both AL and CR mice. Weight loss occurred in shaved animals from both groups (Figure 7A;  $p \leq 0.001$ ) despite an increase in food consumption (Figure 7B;  $p < 0.05$ ). Weights were  $53.43 \pm 3.21$  g at the beginning and  $53.15 \pm 3.10$  g at the end of the experiments for AL animals and  $35.98 \pm 0.95$  g at the beginning and  $32.13 \pm 1.02$  g at the end of the 1-month period for CR animals.

Next, dual X-ray absorptiometry scan measurements were used to measure body composition and indicated that, after 1 month without fur, changes occurred in both the AL and CR groups, but through distinct mechanisms (Figure 7C). Fat area measurements show that this depot is used by AL animals to overcome the increasing thermoregulatory energetic demand imposed by fur coat removal because there is a significant decrease in the relative area occupied by adipose tissue in this

group (Figure 7D;  $p \leq 0.05$ ). CR animals already displayed very modest fat depots before shaving and did not lose a significant amount of this depot (Figure 7D). Instead, CR animals mobilized lean muscle (Figure 7E;  $p \leq 0.001$ ).

To determine whether other organs were subject to energetic recruitment, we weighed them post mortem (Figures 7F–7M). Validating our in vivo measurements, the visceral fat mass was greatly decreased in shaved AL animals and slightly diminished in their CR counterparts (Figure 7F;  $p \leq 0.001$  and  $p \leq 0.05$ , respectively). The soleus muscle mass was decreased only in CR animals after fur coat removal, suggesting muscle utilization in this group (Figure 7G;  $p \leq 0.001$ ). Heart weights increased in both groups after shaving (Figure 7H;  $p \leq 0.001$  and  $p \leq 0.05$  for AL and CR, respectively), possibly because of changes in vasculature and circulation. The spleen and brown adipose tissue (BAT) displayed a curious pattern of decreased mass in AL shaved animals and increased mass in shaved CR mice (Figures 7I and 7J;  $p \leq 0.05$ ). The spleen effect may be related to immune system impairment. Brown fat depots (Figure 7J) may be extended in CR animals to counteract heat loss (Oelkrug et al., 2015). Other organs, such as the liver and kidney (Figure 7K and 7L), as well as the femur (Figure 7M) did not present changes.

Overall, our data suggest that, when the fur coat is removed, CR animals display defective thermoregulation associated with a rupture in locomotion patterns and lean weight loss. These findings are especially significant because they unveil not only a striking effect of CR on the skin but also an adaptive mechanism to cope with reduced insulation derived from skin changes under conditions of reduced caloric intake.

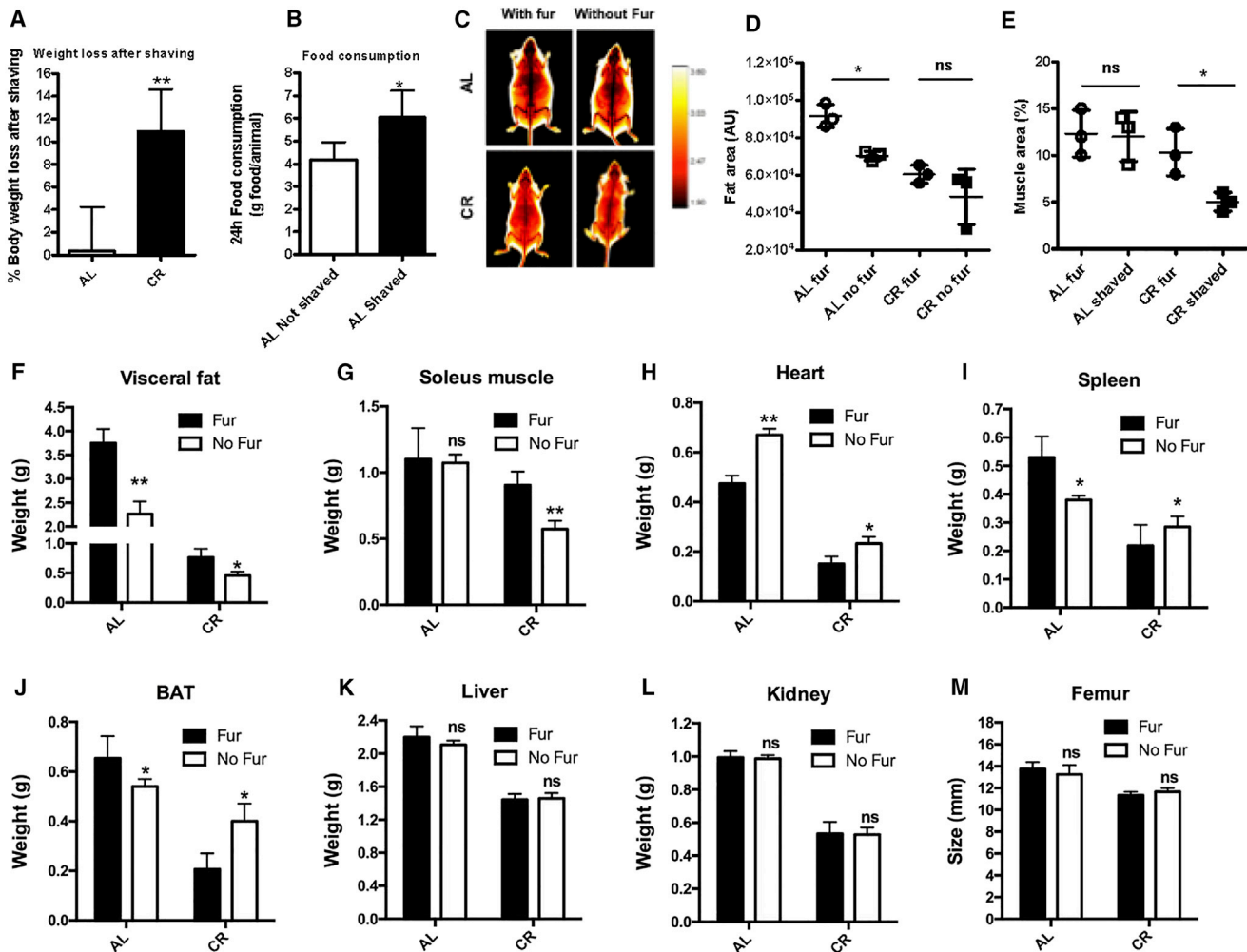


**Figure 7. CR Animals Lose Lean Body Mass in the Absence of Fur**

(A–C) Body weight loss (A), food consumption (B), and body composition (C) 1 month after fur removal.

(D and E) Fat (D) and muscle (E) contents were evaluated using dual X-rays, and their relative area was quantified.

(F–M) The weight and size of several internal organs were assessed after euthanasia: (F) visceral fat, (G) soleus muscle, (H) heart, (I) spleen, (J) brown adipose tissue (BAT), (K) liver, (L) kidney, and (M) femur.

n = 3 independent experiments with 5 animals per group (15 animals). \*p ≤ 0.05, \*\*p ≤ 0.001.

## DISCUSSION

CR is the most studied non-genetic intervention capable of increasing lifespan and healthspan in a plethora of model organisms (McDonald and Ramsey, 2010). In mammals, the shortage in calories elicits compensatory responses (Efeyan et al., 2015) that were thought, until recently, to preserve noble organs (Lusseau et al., 2015). Perhaps because of this assumption, the skin, an organ often thought of as secondary in metabolic regulation, remained unstudied in terms of energy metabolism in response to CR to date.

We focused here on modifications promoted by CR to the skin and found that significant structural and functional changes occur. Some studies demonstrate that CR stimulates respiratory rates in specific tissues by enhancing mitochondrial biogenesis (Tattersall and Milsom, 2003) as well as stimulating uncoupling

between O<sub>2</sub> consumption and oxidative phosphorylation (Tattersall et al., 2006; Zhao and Cao, 2009). In the skin, this metabolic shift occurs in the dermal compartment, where we found that CR induces a more oxidative phenotype (Figure 4). However, the epidermal compartment presents a less prominent oxidative metabolism in CR in a manner not compensated by glycolytic upregulation (Figure 4). This metabolic phenotype has frequently been associated with quiescent stem cells (Ito and Suda 2014) and could be due to the significant expansions in stem cell pools induced by CR in the epidermis (Figure 2). Indeed, the numbers of interfollicular epidermal stem cells were enhanced in CR, which probably accounts for the thicker epidermal layer. The thickening of the epidermis observed in CR (Figure 3) may be functionally significant because epidermis thinning is associated with increased frailty and injury susceptibility in aging (López-Otín et al., 2013). An increase in the hair follicle stem cell pool,

a population of cells involved in fur maintenance, was also observed in CR. Indeed, fur coats were remodeled by CR and presented increased hair growth rates and better hair retention (Figure 3).

Our findings indicating that CR expands stem cell populations in the skin are in line with previous data on other stem cell populations, including intestinal stem cells in mice (Yilmaz et al., 2012) and invertebrates such as *Drosophila* (Rogers and Rogina, 2014). Stem cell pool expansion also occurs in the skeletal muscle of animals exposed to other forms of dietary restriction (Hepple et al., 2006). Interestingly, the stem cell activation status may be more quiescent in CR, a finding in line with the active repression in epithelial cancer incidence observed with this diet (Steinbach et al., 1993; Hursting et al., 2013).

In addition to being controlled by stem cell populations, fur growth also depends on the vasculature. Indeed, vessel sprouting is important to foster nutrient and oxygen supplies in most tissues (Hoeben et al., 2004). In CR animals, hair shaft growth is accompanied by VEGF-related vasculature expansion in the dermal and venule annulus compartments (Figure 3). These changes certainly help provide necessary nutrients for skin remodeling but may represent a burden to CR mice devoid of fur because vasoconstriction and recovery capacities are impaired with this diet (Figure 5), leading to an increase in heat loss and overall energy expenditure.

Globally, we find that CR animals display an array of structural and metabolic alterations that promote changes in heat generation and maintenance. In this regard, it is important to remember that animal housing facilities are generally maintained at temperatures around 22°C, below the thermoneutral range (28°C–31°C) for most murine strains (Ravussin et al., 2012). As a result, mice housed and/or tested in typical laboratory environments, including those in which CR is found to be beneficial, are subjected to cold stress (Ravussin et al., 2012). Interestingly, sweating and panting are not important thermoregulatory mechanisms for rodents, so these animals may rely heavily on their skin and fur for proper thermoregulation (Hart, 1956; Romanovsky, 2014). In the skin, we found that CR predictably decreases dWAT but also leads to epidermal thickening. Although some studies question the importance of dWAT thickness for insulation (Fischer et al., 2016; Abreu-Vieira et al., 2015), the thinner dWAT in the CR animals could have an effect on thermoregulation (Norgan, 1997) because AL skin in the absence of fur was found to be significantly less insulating than CR skin devoid of fur (Figure 5E).

Additionally, the fur in AL and CR animals is markedly different (Figure 1). To verify whether CR-remodeled fur improved thermal insulation, we performed thermographic measurements of surface temperatures in the AL and CR groups in the presence and absence of pelage (Blumberg et al., 2002; Scott et al., 2008; Tattersall et al., 2006, 2009). Our results (Figure 5A) show that heat loss is equal in AL and CR animals in the presence of fur but that CR animals lose considerably higher amounts of heat when devoid of fur. This result suggests that fur remodeling in CR is involved in insulation, although associated changes in blood flow and vasoconstriction are also present and significantly modified by the diet (Figures 5F and 5G). When we evaluated the insulating physical properties of the fur coat in CR

animals, we found that it presents low thermal conductivity, confirming its enhanced insulation properties (Figures 5C–5E). Overall, our data show that compensatory changes in vasculature, skin, and fur thermal isolation occur with CR, resulting in animals that present equal heat loss in the presence of fur but higher heat loss when shaved.

The removal of this remodeled fur coat thus presents a specific challenge for CR animals. Notably, some authors have shown that, under temperature stresses, most insulation occurs via physiological mechanisms, with little contribution from fur or fat (Abreu-Vieira et al., 2015). However, there is also evidence that the fur may be important in rodents: shaved Swiss mice at peak lactation spend more time feeding and increase food intake (Zhao and Cao, 2009), and shaving increases energy expenditure in voles (Kenagy and Pearson, 2000; Szafrńska et al., 2014) and squirrels (Kauffman et al., 2004). Indeed, we found that CR animals present very significant weight loss, mostly because of muscle loss, when shaved (Figure 7). The preferential channeling of excess energy to fat depots instead of muscle in mammals has been extensively documented (Goodman et al., 1980), and the importance of fat depots for individual fitness is also well established (Norgan, 1997). Under increased thermoregulatory demand, these energy depots can be mobilized to generate heat (Dodson et al., 2010; D'Andrea, 2016). In fact, AL animals devoid of fur used fat depots (Figure 7). Nonetheless, the amount of stored fat in CR animals seems to be insufficient to cope with this increased energetic demand, and lean mass consumption (muscle) also takes place (Cahill, 2006). This energy crisis in shaved CR animals is accompanied by a disruption in locomotion pattern (Figure 6) that, in wildlife, would probably affect fitness and survival.

In summary, our results show that CR induces significant vasculature, skin, and fur remodeling in mice, generating a coat with better thermoregulatory properties that compensates for enhanced heat loss without it. An increased pool of hair follicle stem cells accompanies these phenotypic alterations, and probably sustains them, along with an increase in VEGF-mediated dermis-associated vasculature and a bioenergetic shift in both the epidermis and dermis. This could be an evolutionarily selected mechanism that couples skin stem cell plasticity to a thermoregulatory adaptation that allows mammals to increase their fitness and thrive under conditions of caloric limitation.

## EXPERIMENTAL PROCEDURES

### Animals and Dietary Interventions

The experiments were conducted in agreement with the NIH guidelines for humane treatment of animals and were reviewed and approved by the Animal Care and Use Committee (permit number 2013/17). For long-term studies, female 8-week-old Swiss mice were separated into two groups: AL, fed AL with an AIN-93-M diet, and CR, fed daily with 60% of a diet supplemented with micronutrients to reach the vitamin and mineral levels consumed by AL animals (Table S2; Rhooster Lab, Campinas, Brazil). Body mass and food consumption were recorded weekly (Figure S1). Food was offered to CR groups at the same time daily (9:00/11:00 a.m.), and the CR feeding amount was weight-adjusted weekly based on AL food consumption measured 1 week prior. The animals were lodged at 22°C, five individuals per cage, in 12-hr light/dark cycles, and given water *ad libitum*. After 6 months, mice were euthanized after 12 hr of overnight fasting, and tissues were dissected and weighed.

### Back Skin Hair Follicle Evaluation

A 0.5-cm<sup>2</sup> area was shaved, and the follicles were manually sorted and identified using a magnifying glass. The back skin hair follicle types (guard, awl, au-chene, and zigzag) were differentiated by length of the hair shaft, number of medulla cells, and presence of kinks (bends; Müller-Röver et al., 2001). The procedure was conducted in a double-blind manner by two independent counters. Guard hair follicle length was also measured.

### Flow Cytometry

Back skins for hair follicle stem cell isolation and staining protocols were prepared as described previously (Forni et al., 2015). Subcutaneous fat was removed with a scalpel, and the whole skin was placed dermis-down on trypsin (Gibco) at 37°C for 30 min. Single-cell suspensions were obtained by scraping the skin gently to remove the epidermis. The cells were then filtered with strainers (70 μm followed by 40 μm). After blocking with 2% BSA in phosphate-buffered saline (PBSA), cell suspensions were incubated with antibodies for 30 min on ice: α6 integrin (eBioscience, phycoerythrin [PE]-conjugated), CD34 (eBioscience, Alexa Fluor 647-conjugated), CD29 (eBioscience, PE-conjugated) (Table S3). Negative controls comprised of the same class of immunoglobulin G (IgG) isotype controls. Unbound antibodies were washed out through two cycles of PBSA washes, and cells were analyzed using a BD FACSAria II flow cytometer. Data were analyzed and compensated using FlowJo TriStar V10, and at least 50,000 events per sample were collected.

### Hair Growth and Permanence

AL and CR (6-month treatment) back skin hair was trimmed with electric clippers, and active follicle growth (anagen) was observed by hair regrowth measurements. Animals were checked weekly, and areas that entered anagen were quantified in comparison with the original shaved area. Skin regions that had entered anagen (based on regrowth) were photographed, digitalized, and analyzed using ImageJ. Images of each time point were segmented, and the area and number of anagen regions were calculated and corrected for the 2D area of back skin at the original data point. To assess hair follicle tissue permanence, animals had the back skin area colored with a permanent hair dye. The analysis performed was similar to that cited above, following the fading of the dye color through pixel color intensity using ImageJ.

### Histology and Immunofluorescence

Back skin tissues were trimmed and fixed in 4% (w/v) paraformaldehyde. They were then embedded in optimal cutting temperature compound and frozen. After cryosectioning (10–12 μm), they were subjected to immunofluorescence microscopy or H&E staining (Schepeler et al., 2014). The antibodies and their dilutions are shown in Table S3. Secondary antibodies conjugated to Alexa 488 and Alexa 647 (Molecular Probes) were used for imaging. Nuclei were stained using DAPI. Imaging was performed using a Zeiss LSM 510-Meta laser-scanning confocal microscope. Figures were prepared using ImageJ.

### Western Blots

Total proteins from cell lysates were diluted in Laemmli sample buffer (100 mM Tris-HCl, 2% w/v SDS, 10% v/v glycerol, and 0.1% bromophenol blue) containing 100 mM DTT. After heating at 90°C for 5 min, equal amounts of protein, determined through Bradford quantification, were separated by SDS-PAGE and transferred onto nitrocellulose membranes. After membranes were blocked with 5% BSA, detection of individual proteins was carried out by blotting with specific primary antibodies (Table S3). Near-infrared detection using a secondary antibody linked to an infrared dye (LI-COR Biosciences) was used and quantitated with LI-COR Odyssey software. Signals were analyzed by densitometry using ImageJ, and the proteins were normalized either to actin or the stated reference.

### OCRs and ECARs

OCRs were measured in primary cultures using an XF24 Bioanalyzer (Seahorse Bioscience) as described previously (Forni et al., 2016). An assay medium composed of 114 mM NaCl, 4.7 mM KCl, 1.2 mM KH<sub>2</sub>PO<sub>4</sub>, 1.16 mM MgSO<sub>4</sub>, 2.5 mM CaCl<sub>2</sub> (pH 7.2), and 10 mM glucose was used. Cells were seeded in an XF24 24-well microplate at 60,000 cells/well (0.32-cm<sup>2</sup> growth

area) in 500 μL of growth medium and incubated overnight at 37°C in a humidified atmosphere of 95% air and 5% CO<sub>2</sub>. Before the assay, the medium was replaced with 500 μL assay medium. Cells were preincubated for 1 hr at 37°C in air. ATP production-linked O<sub>2</sub> consumption was determined by addition of oligomycin (0.5 μg/mL). After 3 measurement cycles, 5 μM of the uncoupler CCCP was added to determine the maximal respiratory capacity. After a further 3 cycles of measurement, 1 μM rotenone and 1 μM antimycin A were added, ablating mitochondrial O<sub>2</sub> consumption. All respiratory modulators were used at concentrations determined through preliminary titration experiments to determine the ideal quantities for the cell types used.

### Infrared Thermal Imaging

Mice were anesthetized (mask inhalation of isoflurane vaporized in a N<sub>2</sub>/O<sub>2</sub> mixture at concentrations of up to 4% in the induction phase and at 0.8%–1.3% during prolonged experiments) and placed on a tray covered with black thermoneutral paper. The first thermographic score was initiated 10 minutes later to discard any human temperature interference during the thermal imaging acquisition protocol. The dorsal temperature was measured by infrared (IR) thermal images (thermograms) obtained using an IR-sensitive camera (FLIR SC 660). This device produces a 12-bit image (640 × 480 pixels) and stores the temperature information for each pixel with 0.1°C resolution. The technique detects IR wavelength electromagnetic radiation (8–12 μm). We assumed an emissivity of 0.95, as estimated for biological tissues (Scott et al., 2008; Tattersall et al., 2009). All readings were automatically corrected for a non-black body. IR thermal images were analyzed with FLIR Research IR professional analyzing software.

### Thermal Conductivity and Insulating Properties of the Hair Coat and Whole Skin

A temperature recording system was created using a customizable Arduino platform. A negative temperature coefficient (NTC) thermistor with a 3950K beta factor and a nominal resistance of 10 kilo-ohms (kΩ) was used for fur conductivity quantifications. Temperatures were recorded in isoflurane-anesthetized live animals at 15-ms intervals. Five measurements were averaged for a total time of 5 min for each sensor position, either below or above the fur coat. Temperatures were corrected using the Steinhart-Hart equation. Temperatures in the “above” sensor were subtracted from temperatures of the “below” sensor to account for temperature differences promoted by the air layer trapped in the pelage. Measurements were also conducted ex vivo, for whole skin conductivity quantification, with and without fur. Animals were euthanized, and the back skin was immediately dissected and placed on a conical device on top of a Benchmark digital hotplate stirrer used as a stable heat source. The first measurements were made with fur; after hair clipping, measurements were made again without fur. Two LM35 sensors were used to record temperatures every 20 ms; eight measurements were used to calculate mean values. Mean values for the sensor above the skin were subtracted from the ones near the heat source and presented as changes in temperature. Electronic components were measured, and temperatures were calibrated using a Minipa ET-1110DMM digital multimeter with a Type K thermocouple.

### Laser Doppler Measurements of Peripheral Skin Blood Flow

A laser Doppler perfusion monitor (Moor Instruments, Axminster, UK) with a satellite unit detecting flux using a laser probe was adapted from Seabra et al. (2004) and Vercelino et al. (2013). Animals were anesthetized using isoflurane. After shaving the back skin area, laser Doppler probes were secured to the overlying skin. Cutaneous blood flow, measured as red blood cell flux, was used as an index of peripheral circulation. Recordings were displayed continuously by moorLAB v1.31 for Windows. At 1-s intervals, real-time mean blood flow was recorded. After monitoring for 300 s, a single dose of epinephrine (0.2 μg in 20 μL) was applied subcutaneously approximately 3 cm from the probe site (Holloway, 1980), and 100 s were recorded as the stimulated period. The remaining 200 s were recorded as the recovery period.

### Indirect Calorimetry

O<sub>2</sub> consumption (VO<sub>2</sub>) and CO<sub>2</sub> production were measured using a customized, high-precision, single-chamber indirect calorimeter (Columbus

Instruments; Even et al., 1994; Meyer et al., 2015). Each mouse was acclimated to an individual metabolic chamber 1 day before the measurements. Chambers were kept at 22°C with 12-hr light/dark cycles. CR mice were fed 1 hr after the beginning of the light cycle. Thermogenesis was calculated from O<sub>2</sub> consumption and CO<sub>2</sub> production. Calibration was performed before each measurement using primary standard gases. The chamber lid was sealed, and room air was pumped through the chamber at atmospheric pressure at 0.8 L/min. Data were collected every 20 min for 24 hr, with each data point identified by a time stamp. After 24 hr, hair trimming experiments were conducted. Another 24 hr were recorded without the fur coat.

### SPA Measurements

SPA was measured simultaneously with calorimetry. The metabolic chamber was equipped with IR photocell sensors (OptoVarimex, Columbus Instruments). Measurements were performed using customized, high-precision racks of collimated IR activity sensors placed around the acrylic chamber. There were 45 collimated beams crossing the 30-cm-diameter cage, allowing detection of 1-cm movement in three orthogonal axes. Photosensors registered an activity unit each time a beam was interrupted. Physical activity was detected simultaneously on all three axes: forward and backward (x), side to side (y), and up and down (z). SPA was added for every minute.

### Dual X-Ray Absorptiometry Measurements

Mice were scanned 1 month after hair trimming using the FX Pro in vivo imaging system (Akron, Ohio, USA). A combination of xylazine (10 mg/kg) and ketamine (90 mg/kg) was used for sedation. The animals were scanned in a prone position with extended extremities. Fat mass and lean body mass (muscle) were measured in the abdomen (top of the pelvis to the lowermost rib) and whole body (excluding the head). The percentage of abdominal fat was calculated as abdominal fat content divided by total abdomen tissue content. The percentage of total body fat was calculated as total body fat content divided by total body tissue content. The muscle section was evaluated in the lower paws.

### Animal and Organ Weights

We observed recommendations from the Society of Toxicologic Pathology. The animal necropsy order was randomized to prevent bias, and the necropsy order was maintained to obtain meaningful organ weight data. Organs were isolated, and all extraneous tissues (e.g., fat) were removed. Fresh organ weight was determined immediately. Paired organs were weighed together. Terminal body weight was collected at necropsy to control for potential variations induced by novel and stressful handling and diurnal fluctuations (Sellers et al., 2007; Mann et al., 2014).

### Statistical Analysis and Art

Data were analyzed using GraphPad Prism and Origin softwares. Figures represent averages ± SEM of 3–12 measurements and were compared using ANOVA. Two-tailed p values under 0.05 were considered significant. Servier Medical Art and Mind the Graph templates were used.

### SUPPLEMENTAL INFORMATION

Supplemental Information includes Supplemental Experimental Procedures, four figures, and three tables and can be found with this article online at <http://dx.doi.org/10.1016/j.celrep.2017.08.052>.

### AUTHOR CONTRIBUTIONS

M.F.F. was responsible for the concept and design, data collection and/or assembly of data, data analysis and interpretation, and final manuscript approval. J.P. and J.S. were responsible for data collection and/or assembly of data, data analysis and interpretation, and final manuscript approval. T.T.B. and J.E.O.C. were responsible for data collection and/or assembly of data and final manuscript approval. C.A.N. and N.O.S.C. were responsible for data analysis and interpretation and final manuscript approval. A.J.K.

was responsible for concept and design, financial support, data analysis and interpretation, study material provision, and final manuscript approval.

### ACKNOWLEDGMENTS

The authors thank Silvania M.P. Neves, Renata S. Fontes, Flavia M.P. Ong, and Maria de Fatima Rodrigues for excellent animal care and Camille Caldeira for efficient lab management. The authors are also in debt to Prof. Ricardo Giordano for antibody donation and Dr. Marina Burgos-Silva and Angela Castoldi for help with the calorimeter. We acknowledge the kindness of Prof. Marcelo Ganzarolli de Oliveira and Scheila D.F. Alves for help with laser Doppler experiments, as well as Bruno Chausse and Jose Carlos de Lima, Jr., for help with animal transportation and logistics.

This work was supported by grants from FAPESP (10/51906-1), Centro de Pesquisa e Desenvolvimento em Processos Redox em Biomedicina (CEPID Redoxoma, 13/07937-8), a FAPESP PD fellowship (13/04871-6 to M.F.F.), a FAPESP IC fellowship (14/17270-3 to J.P.), FAPESP 12/02270-2 (to N.O.S.C. and T.T.B.), and FAPESP 2014/16320-7 (to C.A.N.).

Received: August 19, 2016

Revised: June 9, 2017

Accepted: August 16, 2017

Published: September 12, 2017

### REFERENCES

- Abreu-Vieira, G., Xiao, C., Gavrilova, O., and Reitman, M.L. (2015). Integration of body temperature into the analysis of energy expenditure in the mouse. *Mol. Metab.* 4, 461–470.
- Alexander, C.M., Kasza, I., Yen, C.L., Reeder, S.B., Hernando, D., Gallo, R.L., Jahoda, C.A., Horsley, V., and MacDougald, O.A. (2015). Dermal white adipose tissue: a new component of the thermogenic response. *J. Lipid Res.* 56, 2061–2069.
- Arwert, E.N., Hoste, E., and Watt, F.M. (2012). Epithelial stem cells, wound healing and cancer. *Nat. Rev. Cancer* 12, 170–180.
- Blumberg, M.S., Lewis, S.J., and Sokoloff, G. (2002). Incubation temperature modulates post-hatching thermoregulatory behavior in the Madagascar ground gecko, *Paroedura pictus*. *J. Exp. Biol.* 205, 2777–2784.
- Bruss, M.D., Thompson, A.C., Aggarwal, I., Khambatta, C.F., and Hellerstein, M.K. (2011). The effects of physiological adaptations to calorie restriction on global cell proliferation rates. *Am. J. Physiol. Endocrinol. Metab.* 300, E735–E745.
- Cahill, G.F., Jr. (2006). Fuel metabolism in starvation. *Annu. Rev. Nutr.* 26, 1–22.
- Cannon, B., and Nedergaard, J. (2011). Nonshivering thermogenesis and its adequate measurement in metabolic studies. *J. Exp. Biol.* 214, 242–253.
- Cotsarelis, G. (2006). Epithelial stem cells: a folliculocentric view. *J. Invest. Dermatol.* 126, 1459–1468.
- D'Andrea, S. (2016). Lipid droplet mobilization: The different ways to loosen the purse strings. *Biochimie* 120, 17–27.
- Dodson, M.V., Hausman, G.J., Guan, L., Du, M., Rasmussen, T.P., Poulos, S.P., Mir, P., Bergen, W.G., Fernyhough, M.E., McFarland, D.C., et al. (2010). Lipid metabolism, adipocyte depot physiology and utilization of meat animals as experimental models for metabolic research. *Int. J. Biol. Sci.* 6, 691–699.
- Driskell, R.R., Clavel, C., Rendl, M., and Watt, F.M. (2011). Hair follicle dermal papilla cells at a glance. *J. Cell Sci.* 124, 1179–1182.
- Driskell, R.R., Jahoda, C.A., Chuong, C.M., Watt, F.M., and Horsley, V. (2014). Defining dermal adipose tissue. *Exp. Dermatol.* 23, 629–631.
- Efeyan, A., Comb, W.C., and Sabatini, D.M. (2015). Nutrient-sensing mechanisms and pathways. *Nature* 517, 302–310.
- Even, P.C., Mokhtarian, A., and Pele, A. (1994). Practical aspects of indirect calorimetry in laboratory animals. *Neurosci. Biobehav. Rev.* 18, 435–447.

- Fischer, A.W., Csikasz, R.I., von Essen, G., Cannon, B., and Nedergaard, J. (2016). No insulating effect of obesity. *Am. J. Physiol. Endocrinol. Metab.* *311*, 202–213.
- Forni, M.F., Ramos Maia Lobba, A., Pereira Ferreira, A.H., and Sogayar, M.C. (2015). Simultaneous isolation of three different stem cell populations from murine skin. *PLoS ONE* *10*, e0140143.
- Forni, M.F., Chausse, B., Peloggia, J., and Kowaltowski, A.J. (2016). Bioenergetic profiling in the skin. *Exp. Dermatol.* *25*, 147–148.
- Fuchs, E. (2015). Cell biology: More than skin deep. *J. Cell Biol.* *209*, 629–631.
- Goodman, M.N., Larsen, P.R., Kaplan, M.M., Aoki, T.T., Young, V.R., and Rudermand, N.B. (1980). Starvation in the rat. II. Effect of age and obesity on protein sparing and fuel metabolism. *Am. J. Physiol.* *239*, 277–286.
- Guarente, L. (2008). Mitochondria—a nexus for aging, calorie restriction, and sirtuins? *Cell* *132*, 171–176.
- Hart, J.S. (1956). Seasonal changes in insulation of the fur. *Can. J. Zool.* *34*, 53–57.
- Hepple, R.T., Baker, D.J., McConkey, M., Muryka, T., and Norris, R. (2006). Caloric restriction protects mitochondrial function with aging in skeletal and cardiac muscles. *Rejuvenation Res.* *9*, 219–222.
- Hoeben, A., Landuyt, B., Highley, M.S., Wildiers, H., Van Oosterom, A.T., and De Bruijn, E.A. (2004). Vascular endothelial growth factor and angiogenesis. *Pharmacol. Rev.* *56*, 549–580.
- Holloway, A. (1980). Cutaneous blood flow response to injection trauma measured by laser doppler velocimetry. *J. Invest. Dermatol.* *74*, 1–4.
- Hsu, Y.C., Li, L., and Fuchs, E. (2014). Emerging interactions between skin stem cells and their niches. *Nat. Med.* *20*, 847–856.
- Hursting, S.D., Dunlap, S.M., Ford, N.A., Hursting, M.J., and Lashinger, L.M. (2013). Calorie restriction and cancer prevention: a mechanistic perspective. *Cancer Metab.* *1*, 10.
- Ito, K., and Suda, T. (2014). Metabolic requirements for the maintenance of self-renewing stem cells. *Nat. Rev. Mol. Cell Biol.* *15*, 243–256.
- Kasza, I., Suh, Y., Wollny, D., Clark, R.J., Roopra, A., Colman, R.J., MacDougald, O.A., Shedd, T.A., Nelson, D.W., Yen, M.J., et al. (2014). Syndecan-1 is required to maintain intradermal fat and prevent cold stress. *PLoS Genet.* *10*, e1004514.
- Kauffman, A.S., Paul, M.J., and Zucker, I. (2004). Increased heat loss affects hibernation in golden-mantled ground squirrels. *Am. J. Physiol. Regul. Integr. Comp. Physiol.* *287*, R167–R173.
- Kenagy, G.J., and Pearson, O.P. (2000). Life with fur and without: experimental field energetics and survival of naked meadow voles. *Oecologia* *122*, 220–224.
- Liu, L., and Shi, G.P. (2012). CD31: beyond a marker for endothelial cells. *Cardiovasc. Res.* *94*, 3–5.
- López-Otín, C., Blasco, M.A., Partridge, L., Serrano, M., and Kroemer, G. (2013). The hallmarks of aging. *Cell* *153*, 1194–1217.
- Lusseau, D., Mitchell, S.E., Barros, C., Deros, D., Green, C., Chen, L., Han, J.D., Wang, Y., Promislow, D.E., Douglas, A., and Speakman, J.R. (2015). The effects of graded levels of calorie restriction: IV. Non-linear change in behavioural phenotype of mice in response to short-term calorie restriction. *Sci. Rep.* *5*, 13198.
- Mann, A., Thompson, A., Robbins, N., and Blomkalns, A.L. (2014). Localization, identification, and excision of murine adipose depots. *J. Vis. Exp.* *2014*. <http://dx.doi.org/10.3791/52174>.
- McDonald, R.B., and Ramsey, J.J. (2010). Honoring Clive McCay and 75 years of calorie restriction research. *J. Nutr.* *140*, 1205–1210.
- Meyer, C.W., Reitmeir, P., and Tschöp, M.H. (2015). Exploration of energy metabolism in the mouse using indirect calorimetry: Measurement of Daily Energy Expenditure (DEE) and Basal Metabolic Rate (BMR). *Curr. Protoc. Mouse Biol.* *5*, 205–222.
- Mihaylova, M.M., Sabatini, D.M., and Yilmaz, O.H. (2014). Dietary and metabolic control of stem cell function in physiology and cancer. *Cell Stem Cell* *14*, 292–305.
- Müller-Röver, S., Handjiski, B., van der Veen, C., Eichmüller, S., Foitzik, K., McKay, I.A., Stenn, K.S., and Paus, R. (2001). A comprehensive guide for the accurate classification of murine hair follicles in distinct hair cycle stages. *J. Invest. Dermatol.* *117*, 3–15.
- Nedergaard, J., and Cannon, B. (2013). How brown is brown fat? It depends where you look. *Nat. Med.* *19*, 540–541.
- Nisoli, E., Clementi, E., Moncada, S., and Carruba, M.O. (2004). Mitochondrial biogenesis as a cellular signaling framework. *Biochem. Pharmacol.* *67*, 1–15.
- Norgan, N.G. (1997). The beneficial effects of body fat and adipose tissue in humans. *Int. J. Obes. Relat. Metab. Disord.* *21*, 738–746.
- Oelkrug, R., Polymeropoulos, E.T., and Jastroch, M. (2015). Brown adipose tissue: physiological function and evolutionary significance. *J. Comp. Physiol. B* *185*, 587–606.
- Partridge, L., and Gems, D. (2002). Mechanisms of ageing: public or private? *Nat. Rev. Genet.* *3*, 165–175.
- Ravussin, Y., LeDuc, C.A., Watanabe, K., and Leibel, R.L. (2012). Effects of ambient temperature on adaptive thermogenesis during maintenance of reduced body weight in mice. *Am. J. Physiol. Regul. Integr. Comp. Physiol.* *303*, R438–R448.
- Rogers, R.P., and Rogina, B. (2014). Increased mitochondrial biogenesis preserves intestinal stem cell homeostasis and contributes to longevity in *Drosophila* mutant flies. *Aging (Albany NY)* *6*, 335–350.
- Romanovsky, A.A. (2014). Skin temperature: its role in thermoregulation. *Acta Physiol. (Oxf.)* *210*, 498–507.
- Roth, G.S., Mattison, J.A., Ottinger, M.A., Chachich, M.E., Lane, M.A., and Ingram, D.K. (2004). Aging in rhesus monkeys: relevance to human health interventions. *Science* *305*, 1423–1426.
- Schepeler, T., Page, M.E., and Jensen, K.B. (2014). Heterogeneity and plasticity of epidermal stem cells. *Development* *141*, 2559–2567.
- Schlacke, T. (2007). Determination of hair structure and shape. *Semin. Cell Dev. Biol.* *18*, 267–273.
- Scott, G.R., Cadena, V., Tattersall, G.J., and Milsom, W.K. (2008). Body temperature depression and peripheral heat loss accompany the metabolic and ventilatory responses to hypoxia in low and high altitude birds. *J. Exp. Biol.* *211*, 1326–1335.
- Seabra, A.B., Fitzpatrick, A., Paul, J., De Oliveira, M.G., and Weller, R. (2004). Topically applied S-nitrosothiol-containing hydrogels as experimental and pharmacological nitric oxide donors in human skin. *Br. J. Dermatol.* *151*, 977–983.
- Sellers, R.S., Morton, D., Michael, B., Roome, N., Johnson, J.K., Yano, B.L., Perry, R., and Schafer, K. (2007). Society of Toxicologic Pathology position paper: organ weight recommendations for toxicology studies. *Toxicol. Pathol.* *35*, 751–755.
- Sohal, R.S., and Weindruch, R. (1996). Oxidative stress, caloric restriction, and aging. *Science* *273*, 59–63.
- Speakman, J.R. (2013). Measuring energy metabolism in the mouse - theoretical, practical, and analytical considerations. *Front. Physiol.* *4*, 34.
- Speakman, J.R., and Mitchell, S.E. (2011). Calorie restriction. *Mol. Aspects Med.* *32*, 159–221.
- Steinbach, G., Kumar, S.P., Reddy, B.S., Lipkin, M., and Holt, P.R. (1993). Effects of caloric restriction and dietary fat on epithelial cell proliferation in rat colon. *Cancer Res.* *53*, 2745–2749.
- Szafrańska, P.A., Zub, K., Wieczorek, M., Książek, A., Speakman, J.R., and Konarzewski, M. (2014). Shaving increases daily energy expenditure in free-living root voles. *J. Exp. Biol.* *217*, 3964–3967.
- Tattersall, G.J., and Milsom, W.K. (2003). Transient peripheral warming accompanies the hypoxic metabolic response in the golden-mantled ground squirrel. *J. Exp. Biol.* *206*, 33–42.
- Tattersall, G.J., Eterovick, P.C., and de Andrade, D.V. (2006). Tribute to R. G. Boulter: skin colour and body temperature changes in basking *Bokermannohyla alvarengai* (Bokermann 1956). *J. Exp. Biol.* *209*, 1185–1196.
- Tattersall, G.J., Andrade, D.V., and Abe, A.S. (2009). Heat exchange from the toucan bill reveals a controllable vascular thermal radiator. *Science* *325*, 468–470.

- Terrien, J., Perret, M., and Aujard, F. (2011). Behavioral thermoregulation in mammals: a review. *Front. Biosci. (Landmark Ed.)* 16, 1428–1444.
- Vercelino, R., Cunha, T.M., Ferreira, E.S., Cunha, F.Q., Ferreira, S.H., and de Oliveira, M.G. (2013). Skin vasodilation and analgesic effect of a topical nitric oxide-releasing hydrogel. *J. Mater. Sci. Mater. Med.* 24, 2157–2169.
- Watt, F.M. (2014). Mammalian skin cell biology: at the interface between laboratory and clinic. *Science* 346, 937–940.
- Yilmaz, O.H., Katajisto, P., Lamming, D.W., Gültekin, Y., Bauer-Rowe, K.E., Sengupta, S., Birsoy, K., Dursun, A., Yilmaz, V.O., Selig, M., et al. (2012). mTORC1 in the Paneth cell niche couples intestinal stem-cell function to calorie intake. *Nature* 486, 490–495.
- Zhao, Z.J., and Cao, J. (2009). Effect of fur removal on the thermal conductance and energy budget in lactating Swiss mice. *J. Exp. Biol.* 212, 2541–2549.